Source apportionment and wet deposition of atmospheric poly- and per-fluoroalkyl substances in a metropolitan city centre of southwest China

Fengwen Wang[a*], Weiru Wang[ab], Daiyin Zhao[a], Jiaxin Liu[c], Peili Lu[a], Neil L. Rose[d], Gan Zhang[b]

[a]State Key Laboratory of Coal Mine Disaster Dynamics and Control, Department of Environmental Science, Chongqing University, Chongqing 400030, China

[b]Guangzhou Institute of Geochemistry, Chinese Academy of Sciences, Guangzhou 510640, China

[c]Chongqing University Cancer Hospital, Chongqing University, Chongqing 400030, China

[d]Environmental Change Research Centre, University College London, Gower Street, London WC1E 6BT, United Kingdom

[*]Corresponding author: fengwenwang@cqu.edu.cn

Abstract

Sixty rainwater samples were collected covering four seasons from July 2020 to April 2021 from the center of Chongqing, a metropolitan city of southwest China, using automatic deposition sampler. The samples were analysed for 17 targeted poly- and per-fluoroalkyl substances (PFASs) by HPLC-MS/MS. The concentration of PFASs ranged from 3.31 ng/L to 196.14 ng/L and dominated by perfluoro-n-octanoic acid (PFOA), perfluoro-n-hexanoic acid (PFHxA), perfluoro-n-butanoic acid (PFBA) and sodium perfluoro-1-octanesulfonate (PFOS). The seasonal variations of dissolved and particulate PFAS were distinct, with the highest level in summer and autumn,

respectively. Positive matrix factorization (PMF) and a wet deposition model were performed to apportion the sources and estimate the wet deposition flux of the 17 PFASs, respectively. PMF analysis indicated that, based on yearly average, paper packaging production (37.4%) and aqueous film forming foam (AFFF) usage (29.8%) were the two major sources, followed by textile production (16.7%) and electronic product manufacturing (16.1%). The highest source contributor for PFASs in winter was AFFF usage (47.0%); while in the other three seasons, it was paper packaging production that contributed the most (50.1%, 39.8% and 34.8% respectively). Seasonal average wet deposition flux of PFASs was estimated to be 13.9 ng/m^2/day. The dry deposition of PFASs was estimated to account for 15.8% of the total atmospheric deposition flux, suggesting a more important role for wet deposition. The results of this study provide important information for understanding of PFASs occurrence and atmospheric wet deposition in Chongqing, and other urban centers across China.

Keywords: source apportionment; Wet deposition; PFASs; Metropolitan city centre

1. Introduction

Poly- and perfluoroalkyl substances (PFASs) are a family of fluorine-containing synthetic persistent organic pollutants (Giesy et al., 2002) which are divided into two main categories: perfluorosulfonic acids (PFSAs) and perfluorocarboxylic acids (PFCAs). According to Lindstrom et al. (2011) and Buck et al. (2021), there were more than 200 industrial products and consumer products containing PFASs. In China, the textile, leather and paper production have produced a large number of PFASs since

2003. In 2006, fifteen enterprises produced more than 200 tons of sodiumperfluoro-1-octanesulfonate (PFOS), and in 2010, the associated PFOS output was more than 1 million tons (Zhou et al., 2016). In 2014, limited use of PFOS and its related compounds took effect in China (Mee, 2019). But short-chain substances including perfluoro-n-butanoicacid (PFBA), potassiumperfluoro-1-butanesulfonate (PFBS) and perfluoro-n-hexanoicacid (PFHxA) have gradually become substitutes for long-chain PFASs and are used in large amounts (Li et al., 2020). Due to their persistent, bio-accumulative, toxic and long range transport property, these PFASs, once emitted, would be ubiquitous in the environment, imposing potential threat to human health and ecosystem safety. As a consequence, there has been a significant recent increase in concern regarding these chemicals as well as in environmental PFASs pollution research worldwide (Domingo et al., 2012; Wu et al., 2019; Paragot, et al., 2020).

Chongqing, one of the youngest municipalities in China, is important manufacturing centre of the country. Its rapid increase in population growth, industrialization, and the fast development of its commercial and tourism economies have resulted in high energy consumption, as well as a greater production of PFASs in urban areas. In 2005, the dominate species of PFASs in Chongqing section of Yangtze River was perfluoro-n-octanoicacid (PFOA) (23~35 ng/L) (So et al., 2007), while by 2018, PFOA concentrations had increased to 50 ng/L (Du et al., 2019). Also in 2018, Liu et al. (2020) investigated the concentration and composition of 17 PFASs in fish and sediments along Yangtze River Basin in Chongqing, and found that PFASs ranged

from 4.74 to 68.5 ng/g in fish and from 1.31 to 32.9 ng/g in sediments, respectively. Both were dominated by PFCAs. At present, studies on PFASs in China are mainly focused on mega cities such as Beijing (Wu et al., 2019), Guangzhou (Chen et al., 2019), and traditional industrial cities such as Dalian (Shan et al., 2015) and Tianjin (Yao et al., 2016a). In Southwest China, there were only a few studies of PFASs, most of which have focused on lakes or rivers (Fang et al., 2019a; Sun et al., 2018). Recently, Fang et al. (2019b) investigated the spatial and seasonal pattern of atmospheric perfluoroalkyl acids (PFAAs) at five different areas of Chengdu. However, studies elsewhere are sparse and there have been no reports on the occurrence and sources of PFASs in the atmosphere of Chongqing. In this study, sixty rainwater samples covering four seasons from July 2020 to April 2021 were collected at a core urban site of Chongqing University. These samples were analyzed for 17 PFASs to apportion their sources and estimate wet deposition flux. The study on the pollution characteristics and wet deposition of PFASs is of great importance for understanding the pollution status of regional atmospheric PFASs. Such data are important to establish effective abatement strategies for the prevention of PFASs pollution in Chongqing and other urban areas.

2 Materials and methods

2.1 Sampling area, site and sample collection

The Three Gorges Square in Shapingba District of Chongqing Municipality (hereinafter referred to as "Sha District") was selected as a typical of Chongqing urban area. Sha District, with Jialing River in the east and Jinyun Mountain in the

west, is an important node of “Chongqing westward development strategy”. Various functional areas including industrial area, teaching area and commercial area are distributed in Sha District. The integrated circuit industry accounts for more than 80% of the total product, making it an ideal representative district for assessing atmospheric PFASs pollution. Influenced by the subtropical monsoon climate, the average annual precipitation in Sha District is about 1050 mm, which is mainly concentrated in summer and autumn (Chongqing Shapingba Meteorological Bureau). In this study, the sampling site (29.57° N, 106.46° E) is located on the roof of 5-story building in Chongqing University Campus A, and is shown in Figure 1. This site is 1.3km far away from Sha District Meteorological Bureau. Around this site, there are no high buildings and big trees, making it an ideal observation site for rainwater collection.

An automatic deposition sampler (APS-3A, APS-3A, Changsha Xianglan Scientific Instrument Co., Ltd., China) made of High Density Polyethylene (HDPE) was used to collect the rainwater samples. Before sampling, the PE bucket would be washed with deionized water and rinsed three times using methanol solution. The sampler worked under a moisture sensor: it would open automatically when it rained or snowed and close once the precipitation stopped, thus ensuring only wet deposition would be collected. In brief, precipitation sample began to be collected when it rained and finished when the rain stopped. Sampling duration depended on each rainfall event but did not exceed 23.5h as the sample container was changed each day. Sixty rainwater samples were collected from July 2020 to April 2021. These samples were

allocated to seasons as follows: Summer 2020 (July 26 - September 3, n=7), Autumn 2020 (September 6 - November 2, n=17), Winter 2020 (November 22 - January 24, n=19) and Spring 2021 (February 25 - April 18, n=17). After collection, each rainwater sample was immediately filtered through a GF/F filter (Whatman). The filtered phase on the filter membrane were particulate samples. The rainwater that has been filtered were dissolved samples. The particulate samples were treated on a monthly basis and integrated as a number of ten. Two parallel operational sample blanks were obtained in each season. Rainwater sample blanks were practiced as using MeOH to directly elute the bucket without collecting samples.

2.2 Sample treatment and analytical procedures

5 ng standard samples containing the mass-labeled mixture MPFAC-MXA (Wellington laboratories, Guelph, Canada) was added into the dissolved rainwater sample to indicate the recovery rate. The sample was then shake well and left for 30 min. The anion exchange column (Oasis WAX, purchased from American Water Company) was activated successively with 0.1% ammonia-methanol solution, methanol and pure water (4 mL in each), and the flow rate was controlled at 1-2 drops/s. SPE was then performed at a flow rate of 1-2 drops/s and always keep moist. The WAX column was then flushed with 4 mL 25mM acetate buffer (pH=4) and centrifuged at 6000 r/min for 20 min to remove residual water. Finally, 4 mL methanol and 4 mL methanol of 0.1% ammonia were successively used for solvent elution, and the eluents were collected in a 50 mL PP centrifuge tube. In order to avoid the adsorption of long chain PFASs, the eluent was concentrated to 0.5 mL by soft

nitrogen blow and filtered using 0.22 μm filter. The filtrate was stored in a -20℃ refrigerator for further analysis. 5 ng internal standard containing the isotope-labeled $^{13}C_8$-PFOA (Perfluoro-n-[$^{13}C_8$] octanoic acid, Wellington laboratories, Guelph, Canada) was used as internal standard to quantify the PFASs.

The particulate PFASs samples were freeze-dried for 72 h. They were then cut into pieces with scissors and collected into 50 mL centrifuge tube. Ultrasonic extraction was performed three times with 10 mL methanol. 2 ng standard samples were added into the centrifuge tube before extraction to indicate the recovery rate. The extraction was centrifuged at 7200r/min for 10 min to obtain the supernatant. Then the extract was concentrated to 1 mL under soft nitrogen and further purified by Envi-carb column (Shanghai ANPEL Scientific Instrument Company). HPLC-MS/MS analysis (Shimadzu 8060, Shimadzu Corp; equipped with Kinetex C18 100A column, 2.1 mm × 100 mm, 2.6 μm, Phenomenex Inc.) were as follows. The column temperature was maintained at 30 °C. A flow rate of 0.4 mL/min of binary gradient was used and the sample injection volume was 1 μl. The mobile phase consisted of 5 mM ammonium acetate (phase A) and methanol (phase B), with a flow rate of 0.4 ml/min. The initial proportion of mobile phase was 70% A and 30% B, then phase B was linearly increased to 80% over 4 min and maintained for 5 min. The cycle was completed by returning to the initial percentage (70% A and 30% B) in 0.1 min and stabilized for 5 min to restore the initial conditions before the next injection. The standard samples containing C4-14,16,18 perfluotoalkyl carboxylic acids (PFCAs) and C4,6,8,10 perfluorosulfonic acids (PFSAs) was also purchased from Wellington

laboratories (Guelph, Canada). The targeted 17 PFASs was abbreviated as PFBA, PFPeA, PFHxA, PFHpA, PFOA, PFNA, PFDA, PFUdA, PFDoA, PFTrDA, PFTeDA, PFHxDA, PFODA, PFBS, PFHxS, PFOS and PFDS. The full name of all compounds are provided in Table S1 in supporting information. The MS parameters (voltages, precursor and product ions) for 17 PFASs are provided in Table S2 in supporting information.

2.3 QA/QC

To avoid loss of long chain PFASs due to adsorption, all the chromatographic pipeline and utensils were made of PEEK plastic or stainless steel. All vessels were first rinsed with hot potassium dichromate-sulfuric acid solution, then laid for overnight and washed using 18.2 Ω Milli-Q water. Organic reagents used in laboratory were HPLC grade quality and purchased from Shanghai ANPEL Scientific Instrument Company (HPLC grade, purity: 95%). After sample vessels with aluminum foil, they were put in muffle furnace at 450 °C for 4 hours. All utensils would be rinsed twice with reagents before used. Targeted PFASs compounds were occasionally detected in the procedural blank and nominal detection limits for individual PFASs were summarized in Table S3. The average surrogate recoveries ranged from 42.1%-120.3% for dissolved samples; for particulate PFASs samples, they ranged from 41.1%-113.0%, and were also shown in Table S3. Within each batch of 12 sample analyses a duplicate sample was analysed. All paired duplicate samples agreed to within 15% of the measured values (n=12). The results were displayed as blank correction by subtracting an average blank including laboratory and filed blank

177 from each sample. Reported concentrations here were recovery corrected.

178 **2.4 Air mass back trajectory analysis**

179 Air mass back trajectory was used to trace atmospheric transport pathways. In
180 this study, 24-hour back trajectories at sampling site at 1200 UTC were calculated at
181 100 m above ground level at 1-hour intervals for the sampling days. These air masses
182 were clustered based on the total spatial variances using the TrajStat software to
183 characterize the origins of air masses (Wang et al., 2020). The frequencies of the
184 backwards trajectories were presented as percentages of each cluster.

185 **2.5 PMF modeling**

186 Details of PMF can be found in the EPA PMF 5.0 Fundamentals and User Guide
187 (https://www.epa.gov). In brief, the PMF model is based on the following equation:

188 $$X_{ij} = \sum_{k=1}^{p} G_{ik} F_{kj} + E_{ij} \quad (1)$$

189 Where X_{ij} is the concentration of the j^{th} congener in the i^{th} sample of the original data
190 set; G_{ik} is the contribution of the k^{th} factor to the i^{th} sample; F_{kj} is the fraction of the k^{th}
191 factor arising from congener j; and E_{ij} is the residual between the measured X_{ij} and the
192 estimated X_{ij} using p principal components.

193 $$Q = \sum_{i=1}^{n} \sum_{j=1}^{m} \left(\frac{E_{ij}}{U_{ij}} \right)^2 \quad (2)$$

194 Where U_{ij} is the uncertainty of the j^{th} congener in the i^{th} sample of the original data set
195 containing m congeners and n samples. Q is the weighted sum of squares of differences
196 between the PMF output and the original data set. One of the objectives of PMF analysis
197 is to minimize the Q value.

When X_{ij} < MDL, U_{ij} is calculated as:

$$U_{ij} = 5/6 \times MDL \quad (3)$$

When $X_{ij} \geq$MDL, U_{ij} is calculated as:

$$U_{ij} = \sqrt{(\delta \times c)^2 + (0.5 \times MDL)^2} \quad (4)$$

Where δ is the error coefficient and usually used as value of 0.2. c is the concentration of measured individual PFASs. In this study, the number of factors from 3 to 7 was examined with the optimal number of factors determined from the slope of the *Q* value versus the number of factors. Finally, a 4-factor solution was chosen for the data sets.

2.6 The dissolved-particle partition of PFASs in rainwater

The partitioning coefficient (log K_d) of each PFASs including the PFSAs and PFCAs between dissolved and particulate phase was calculated based on the following equation:

$$\log K_d\ (cm^3/g) = \log(C_{PM}/(A_{PM} \times C_W)) \times 1000 \quad (5)$$

C_{PM} and C_W is the particulate and dissolved concentrations of each monomer (ng/L), and APM is the total particle mass of rainfall (g/L).

2.7 Wet deposition flux estimation

Wet deposition flux (F, ng/m^2/day) were estimated using volume weighted mean (VWM) concentration in rainwater samples (C_{PFAS}, ng/L) and precipitation rates (P, L/m^2/d) obtained from our meteorological instruments (Wujiang Heshun Scientific Company, China) installed at sampling site, which is descripted as:

$$F\ (ng/m^2/day) = C_{PFAS} \times P \quad (6)$$

The precipitation rates, pH and rainwater volume of the samples are summarized in Table S3. The uncertainty of F_{wet} is estimated using the equation below:

$$U_{ij} = (e_j^2 + (d_j \times X_j)^2)^{0.5} \quad (7)$$

Where U_{ij} is the uncertainty, e_j is the detection limit of the instrument, d_j is the coefficient of uncertainty, and X_{ij} is the concentration of the target compound. d_j can be 0.1 or 0.25. For those compounds that are volatile or have secondary generation/loss, d_j could be 0.1 (Anttila et al., 1995; Cheng et al., 2010; Liu et al., 2013). The uncertainty of individual PFASs wet deposition flux ranged from 10.5% to 55.0% in this study.

3 Results and discussion

3.1 Air mass back trajectory conditions

The clustered 24-hour air mass back trajectories from altitudes of 100 m arriving at sampling site during the sampling period are shown in Figure. 2. The total number of 756 air masses could be divided into 6 categories. In summer, the dominant air parcels were from south (28.09%) and southeast (19.49%) and passed over Guizhou province. In autumn, the air parcels were faster than those in summer, making the transport paths relatively short. The air masses were dominated by northeast (22.58%) and easterly airflow (21.04%) and mainly came from the local regions, such as Jiangbei, Fuling and Changshou Districts in Chongqing. In winter, air movement was significantly affected by the topography of the region so the speed of air parcels was

the lowest and the transport pathways were the shortest. The air masses were dominated by the flow from northeast (32.40%) and southeast (18.37%), and mainly originated from the local regions, such as Yubei, Beibei and Banan District in Chongqing. In spring, the air masses were mainly from the east (39.97%) and passed over central Chongqing. Therefore, the atmosphere above the sampling site during the sampling period, in spring and summer, was influenced by regions from Guizhou and Sichuan province. While, in autumn and winter, the air mass was mainly affected by the local Chongqing, characterizing of short circulation pathway.

3.2 Occurrence, composition and seasonal variation of PFASs

The detection efficiency of 17 PFASs are summarized in Table S4. 13 PFASs, including 10 PFCAs and 3 PFSAs, were above detection limits while PFTrDA, PFTeDA, PFODA and PFDS were not. This may be due to the higher degree of fluorination and lower water-solubility of long-chain PFASs ($C \geqslant 8$) making them difficult to evaporate from waterbody into the atmosphere (Lei et al., 2004; Kim et al., 2020). To directly compare the concentration between dissolved and particulate PFASs, the unit of these two type samples were standardized as ng/L as suggested by Shan et al. (2015). Seasonal variation of the concentrations of PFASs in the dissolved and particulate samples (colorful histogram) and the ambient temperatures (solid dot line) are shown in Figure. 3. The concentrations of the individual PFASs over four seasons are in Table S5. The concentrations of dissolved and particulate PFASs were 1.3-191.3 ng/L and 1.00-7.64 ng/L, with mean of 20.3 ng/L and 4.39 ng/L, respectively. A significant seasonal variation in the concentrations of the dissolved

PFASs was observed (Figure 3a) with highest concentrations in summer (average: 31.6 ng/L), and lowest in winter (average: 3.3 ng/L). The concentrations were significantly correlated with ambient temperature and rainfall amount ($p<0.05$). Driven by the high temperature (average 31℃) and strong solar radiation in summer, PFASs and the volatile precursors are more readily converted from particulate into gaseous phase. elevating PFASs concentrations in the dissolved fraction (Yao et al., 2016a). By contrast, there was a long rainfall period in the autumn (2020/9/17-2020/10/05) which lasted for 17 consecutive days, with a total rainfall of 18 mm (Table S6). Such weather conditions are not suitable for PFASs accumulation in the atmosphere. In a survey of precipitation in Dongguan from 2013 to 2017, Chen et al. (2021) found that precipitation with a duration of more than 6 hours resulted in removal efficiency of 40% for atmospheric aerosols. The seasonal trend of particulate PFASs were different from dissolved, higher in autumn and winter (7.64 ng/L and 6.98 ng/L, respectively), lower in spring and summer (1.00 ng/L and 1.93 ng/L, respectively) (Figure 3b). In autumn and winter of Chongqing, rainfall mainly occurs at night, accounting for 65% and 61% of the total precipitation amounts, respectively. Wang et al. (2020) compared the removal effect of night and daytime rainfall with different durations on atmospheric particle in the Pearl River Delta, and found that the removal efficiency of night rain, lasting 7 and 12 hours, was much higher than during the day. The possible reason could be the complicated sources of particles and atmospheric boundary layer conditions at daytime compared with night. Therefore, PFASs distribution in this study could be caused by atmospheric removal of

284 particulate by nighttime rainfall and subsequent gas-particle repartitioning between
285 “aged” particulate and gaseous PFASs.

286 Figure S1 summarize the composition characteristics of PFASs over four seasons.
287 It can be seen that the total PFCAs were higher than PFSAs with the same carbon
288 number. This is consistent with previous studies that was conducted in North America
289 (Scott et al., 2006) and Japan (Taniyasu et al., 2013) and maybe due to the much wider
290 production and application of PFCAs and its precursors than those of PFSAs in China
291 (Han et al., 2019). PFASs were dominated by PFOA, PFHXA, PFBA and PFOS, with
292 average concentration of 12.6, 3.3, 2.7 and 1.2 ng/L, respectively (Figure S1). PFBA
293 contributed 20% of the total PFASs, which was significantly higher than ratio in
294 Shenyang (Liu et al., 2007), but consistent with the composition of indoor dust in
295 Guangzhou and Qingyuan (Zhang et al., 2020). With the introduction of C_4-C_7 PFASs
296 alternatives and the restriction on the use of long-chain, such as PFOS and PFHpA in
297 China, PFBA could gradually become the dominant species of PFASs in atmospheric
298 environment.

299 Table 1 compares the mean concentrations of selected PFASs in rainwater at
300 Chongqing with other places worldwide. The concentration of PFASs in rainwater at
301 Chongqing was higher than those in Hongkong (7.68 ng/L) (Kwok et al., 2010),
302 Beijing (0.23-62.4 ng/L) (Zheng et al., 2020) and Hangzhou (2.85-35.1 ng/L) (Zhang
303 et al., 2017). Compared with those places out of China, such as Toronto (Leo et al.,
304 2017), Maltese Islands (4.05 ng/L) (Sammut et al., 2017), Northern Italy (7.9-28.5
305 ng/L) (Dreyer et al., 2010), and in Lake Huron (maximum: 56.9 ng/L) (Gewurtz et al.,

2019), the concentration of PFASs in rainwater in Chongqing was markedly higher.

3.3 The dissolved-particle partition of PFASs

Compared with the dissolved-particle partition of PFASs in waterbody, there have been few studies on this behavior in rainwater samples. Table 2 summarize the $\log K_d$ (cm^3/g) and associated parameters of 13 PFASs. It can be seen that the $\log K_d$ of C_6-C_{12} PFCAs ranged from 6.6 and 10.3, and the $\log K_d$ of C_4, C_6 and C_8 PFSAs was from 7.2 and 8.9. The $\log K_d$ of short carbon number PFSAs were double those calculated for bothe the waters of Tokyo Dam (Ahrens et al., 2010) and snowfall of northern China (Shan et al., 2015). However, there were not significant differences between them (t-statistical test, p>0.05). Based on in-situ measurement system, Kim et al. (2020) studied the interphase partitioning behavior of atmospheric PFASs and found that the maximum $\log K_d$ could be 4 times the minimum value due to the influence of physical-chemical properties of monomers, particle size distribution and pH of the aqueous phase. Figure S2 shows the variation of 13 PFASs $\log K_d$ along with the carbon chain. The $\log K_d$ of C_4-C_6 PFCAs and C_4, C_6 and C_8 PFSAs increase with the carbon number. PFSAs were generally higher than PFCAs with the same carbon number (i.e., PFBS: 8.3, PFDA: 7.7). The adsorption of PFASs onto particulate matter is affected by types of functional groups, electrostatic interaction, hydrogen bonding and ligand exchange (Higgins et al., 2006). Short-chain PFCAs (C_2-C_6) have strong interaction with minerals and inorganic anions in atmospheric particles, therefore $\log K_d$ was inversely proportional to the carbon chain length (Yao et al., 2016b). Higgins et al., (2006) also found the hydrophobicity of PFASs

increased with the carbon chain length, making them more easily adsorbed by particles. Therefore, the logK_d of C_4-C_8 PFASs was proportional to the carbon chain length.

3.4 Source identification of PFASs using diagnostic ratios and PMF

The diagnostic ratio method has been widely used to identify and characterize PFASs sources at water and soil. There have been seldom study for the ratio method for atmosphere. The diagnostic ratios used here were from Cao et al. (2019), and they were detailed as PFOA/PFNA、PFOS/PFOA and PFHpA/PFOA, respectively. The PFOS/PFOA and PFHpA/PFOA over four seasons were all lower than 1, without obvious seasonal variation. The seasonal trend of PFOA/PFNA was significant, with an average of 20.34, 64.16, 5.99 and 22.65, respectively. According to Chen et al. (2015), when 7 < PFOA/PFNA < 15, it indicates local industrial sources. When PFOA/PFNA is higher than 15, it suggests sources from degradation of PFASs precursors.

To quantitatively estimates the contributions from specific sources, PMF was used to apportion the sources of PFASs on the basis of a yearly distributed datasets. In this study, a 60 × 9 (60 samples with 9 PFASs each) dataset was introduced to the EPA PMF 5.0 model to estimate the source contributions of the 9 PFASs (PFOA、PFBA、PFPeA、PFHxA、PFHpA、PFOS、PFNA、PFDA and PFUdA) with high detection efficiency (85% -100%). A 4-factor solution and 4 kinds of source contributions on whole samples and PMF factor profiles are shown in Figure. 4.

Factor 1 accounted for 37.4% of the sum of the measured 9 PFASs. It has high

loadings of PFOA and PFHxA. PFOA is widely used as an additive in the production of paper food packaging materials (Martínez-Moral et al., 2012) while PFHxA are alternatives to PFOA for coating materials and food/pharmaceutical packaging (Xiao et al., 2012). Since implementation of the 12th Five-Year Plan of Chongqing Culture and Industry, printing has been set as the development goal in the upper reaches of Yangtze River (http://www.chinairn.com/). Thereafter, Yutong Printing was successively introduced into Shapingba Industrial Park. According to NBSC (http://www.stats.gov.cn/english/), Chongqing had almost two hundred printing factories in 2020, a certainly significant use of PFOA by any measure. Therefore, factor 1 is defined as paper packaging production.

Factor 2 contributed 16.1% of the 9 PFASs. PFBA is the main component. PFBA and other short-chain PFCAs are mainly used as synthetic flotation agents of precious metals, antifouling and oil-proof coatings (Qi et al., 2017). In Sha District, electronical industry is one of important parts of the total industry categories. The integrated circuit accounted more than 80% of the total in Chongqing. Hence, Factor 2 could be assigned as electronic product manufacturing.

Factor 3 explained 16.7% of the 9 PFASs. It was mainly dominated by PFDA, PFHxA and PFPeA. PFDA is the main detected substance in textiles. PFPeA is often used as an indicator of the emission source from Teflon emulsifier and textile production. PFHxA is the degradation product of textile raw material FTOHs (Klaunig et al., 2015). Factor 3 is considered as textile production (Liu et al., 2015; Han et al., 2019).

Factor 4 accounted for 29.8% of the 9 PFASs. PFOS, PFHpA and PFUdA were the main components. PFOS and its precursors have been widely used in foam fire extinguishing agents, and the concentration in atmosphere was directly proportion to the amount of their usage. Young et al. (2021) found that the indoor air at fire station was secondary dominated by PFHpA. PFUdA is commonly used as raw material for production of foam extinguishing agent (D'Agostino, et al., 2017). Thus factor 4 was interpreted as foam extinguishing agent (AFFF) usage.

The seasonal contributions of each source to the 9 PFASs are shown in Figure. 5. An obvious seasonal variation could be observed: the highest source contributor for PFASs in winter was aqueous film forming foam (AFFF) usage (47.0%); while in the other three seasons, it was paper packaging production that contributed the most (50.1%, 39.8% and 34.8% respectively). According to the statistics from the Chongqing Fire Network (http://www.cqfire.com/main/), a greater incidence of fire occurred in winter due to inappropriate indoor heating using natural gas or electric heaters. Therefore, the high contributions from AFFF usage could be caused by the intensive application of these agents for the fire extinction. A high frequency of fire drill in public mega bus/railway stations and airports could also contribute to this result. The contribution from electronic product manufacturing in spring (29.9%) was much more than that in summer (7.7%). This is in good agreement with data from the China Business Industry Research Institute (https://s.askci.com/data/year/), which shows that the output from integrated circuit production in spring 2019 in Chongqing was 2.1×10^8 units compared with 1.0×10^8 units in summer. Finally, considering the

high contribution of paper packaging production over the three seasons, it is reasonable to infer that the control and mitigation of PFASs emissions from this industry are necessary for the abatement of atmospheric PFASs in urban Chongqing.

3.5 Wet deposition of PFASs

The wet deposition flux of individual PFASs in rainwater samples over the four seasons are presented in Table 3. The deposition flux of 17 PFASs (ng/m^2/day) ranged from below detection-175.5, with an average of 13.9. The seasonal abundances of 17 PFASs varied significantly with summer (1375.8 ng/m^2/season) > autumn (368.5 ng/m^2/season) > spring (211 ng/m^2/season) > winter (80.2 ng/m^2/season). The flux in summer comprised about 68% of the total annual wet deposition flux. Chongqing is located in the transition zone between plateau and sub-tropical monsoon humid climate and abundant and frequent rainfall occurs each summer. Rainfall in summer can be as high as 343 mm, followed by a sub-peak in rainfall in autumn (18.4 mm) and with lowest rainfall in winter (8.1 mm) (Pu et al., 2021). Therefore, high concentrations of PFASs together with high rainfall in summer could result in highest wet deposition at this time. The wet deposition flux in Chongqing are compared to previously published results as also shown in Table 3. Fluxes in Shenzhen (1162.7 ng/m^2/day), Xiamen (872 ng/m^2/day), Hefei (595 ng/m^2/day) and Nanjing (446 ng/m^2/day) are clearly higher than those for Chongqing (Chen et al., 2019). However, PFASs deposition fluxes (6.8-36.8 ng/m^2/day) at Lake Ontario were found to be lower than those observed in this current study (Gewurtz et al., 2019).

In order to assess the relative contribution of atmospheric dry deposition to the

416 total flux of PFASs, we estimated the dry deposition flux as described below. Chen et
417 al., (2019) found that the gas to liquid distribution ratio of atmospheric PFASs ranged
418 from 1:4-1:9. As discussed above, precipitation data from Chongqing Shapingba
419 Meteorological Bureau show that the highest rainfall period in Chongqing occurs in
420 summer. Therefore, we used a ratio of 1:4 (dry to wet deposition) to estimate the dry
421 deposition flux in spring, autumn and winter; and a ratio of 1:9 in summer. Table S7
422 summarized the estimated dry and annual deposition flux of PFAS and uncertainty.
423 Based on these assumptions, the dry deposition flux of PFASs in this study was
424 estimated to be from NA-22.1 ng/m^2/day and averaged at 2.6 ng/m^2/day. The dry
425 deposition flux of PFASs would therefore account for 15.8% of the total atmospheric
426 deposition flux, suggesting a more important role for wet deposition. Given the
427 estimate of atmospheric wet + dry deposition flux in each season and the 390 km^2 area
428 of Sha district, an estimated 23.5 kg/year PFASs would be deposited to this region in
429 Chongqing.

430 Although this study was limited to four seasonal datasets collected from only one
431 urban site, general information of temporal variation of atmospheric deposition of
432 PFASs at Chongqing could still be obtained. However, these results didn't account for
433 the spatial variation across Chongqing. Larger scale researches using aerosol
434 collecting sampler at multiple sites are needed to reveal the spatial variations of
435 atmospheric dry deposition of PFASs. Further investigation of the continuous study on
436 size distribution, gas-particle partition and direct estimation on dry deposition of
437 atmospheric PFASs in mega Chongqing would be interesting and fruitful.

4 Conclusions

This study provides the first data sets of atmospheric wet deposition of PFASs in urban Chongqing. The seasonal average of dissolved and particulate PFASs in rainwater of urban Chongqing was 20.3 ng/L and 4.39 ng/L, respectively. The concentrations of PFCAs were higher than PFSAs; while the $\log K_d$ of PFSAs were generally higher than PFCAs with the same carbon number. PMF identified that the highest source contributor for PFASs in winter was AFFF usage (47.0%); while in the other three seasons, it was paper packaging production that contributed the most (50.1%, 39.8% and 34.8% respectively). The seasonal wet and dry deposition flux of PFASs was averaged at 13.9 and 2.6 ng/m^2/day, indicating a more important role of atmospheric wet deposition. An estimated ~23.5 kg/year PFASs would be atmospherically deposited to Sha district in Chongqing.

Acknowledgement

This work was funded by the National Natural Science Foundation of China (NSFC) (No: 42077319, 52070025); National Key R&D Program of China (No: 2018YFC0807805；2019YFC1805500); The Fundamental Research Funds for the Central Universities (2020CDCGHJ017); Technological Innovation and Application Development Key Projects of Chongqing Municipality, China (No. cstc2019jscx-gksb0241).

References

Ahrens, L., Taniyasu, S., Yeung, L.W.Y., Yamashita, N., 2010. Distribution of polyfluoroalkyl compounds in water, suspended particulate matter and sediment

460 from Tokyo Bay, Japan. Chemosphere. 79(3):266-272.
461 Anttila, P., Paatero, P., Tapper, U., Jarvinen, O., 1995. Source identification of bulk
462 wet deposition in Finland by positive matrix factorization. Atmos. Environ.
463 29(14):1705-1718.
464 Cao, X.H., Wang, C.C., Lu, Y.L., Zhang, M., Khan, K., Song, S., Wang, P., Wang, C.,
465 2019. Occurrence, sources and health risk of polyfluoroalkyl substances (PFASs)
466 in soil, water and sediment from a drinking water source area. Ecoto. Environ.
467 Safety. 174:208-217.
468 Chen, H., Zhang, L., Li, M.Q., Yao, Y.M., Zhao, Z., Munoz, G., Sun H.W., 2019. Per-
469 and polyfluoroalkyl substances (PFASs) in precipitation from mainland China:
470 Contributions of unknown precursors and short-chain (C2-C3) perfluoroalkyl
471 carboxylic acids. Water Res. 153:169-177.
472 Chen, H.Z., Wu, D., Yuan, Z.Y., 2021. Observational study of PM2.5 scavenging by
473 rain in Dongguan. Acta Scientiae Circumstantiae, 41(5): 1741-1752. (In Chinese)
474 Chen, S., Jiao, X.C., Gai. N., Li, X.J., Wang, X.C., Lu, G.H., 2015. Perfluorinated
475 compounds in soil, surface water, and groundwater from rural areas in eastern
476 China. Environ. Pollut. 211, 124-131.
477 Cheng, Y., Lee, S.C., Ho, K.F., Chow, J.C., Watson, J.G., Louie, P.K.K., Cao, J.J., Hai,
478 X., 2010. Chemically-speciated on-road PM2.5 motor vehicle emission factors in
479 Hong Kong. Sci. Total Environ. 408(7):1621-1627.
480 D'Agostino, L.A., Mabury, S.A., 2017. Certain Perfluoroalkyl and Polyfluoroalkyl
481 Substances Associated with Aqueous Film Forming Foam Are Widespread in

Canadian Surface Waters. Environ. Sci. Technol., 51(23):13603-13613.

Dreyer, A., Matthias, V., Weinberg, I., Ebinghaus, R., 2010. Wet deposition of poly- and perfluorinated compounds in Northern Germany. Environ. Pollut. (158):1221-1227.

Domingo, J.L., Ericson-Jogsten, I., Perello, G., Nadal, M., Van, B., Karrman, A., 2012. Human exposure to perfluorinated compounds in Catalonia, Spain: contribution of drinking water and fish and shellfish. J. Agric. Food Chem. 60(17):4408-4415.

Du, G.Y., Jiang, X, P., Zhuo, L., Shi, Y.G., Ren, M.Z., Cai, F.S., Zheng, J., Zhuang, X., Luo, W.K., 2019. Distribution characteristics and risk assessment of perfluorinated compounds in surface water from Chongqing Section of the Yangtze River. Eco. Environ. Sci. 28(11): 2266-2272. (In Chinese)

Fang, S.H., Li C., Bian, Y.X., Wang, D., Hao, Y.Q., Yin, H.L., Sun, J., 2019a. Pollution characteristics and flux of perfluoroalkyl substances in Minjiang River. China Environ. Sci. 39(7): 2983-2989. (In Chinese)

Fang, S.H., Li, C., Zhu, L.Y., Yin, H.L., Yang, Y.C., Ye, Z.X., Cousins, I.T., 2019b. Spatiotemporal distribution and isomer profiles of perfluoroalkyl acids in airborne particulate matter in Chengdu City, China. Sci. Total Environ. 689:1235-1243.

Gewurtz, S. B., Bradley, L.E., Backus, S., Dove, A., McGoldrick, D., Hung, H., Dryfhout, C.K., 2019. Perfluoroalkyl Acids in Great Lakes Precipitation and Surface Water (2006-2018) Indicate Response to Phase-outs, Regulatory Action, and Variability in Fate and Transport Processes. Environ. Sci. Technol.

504 53(15):8543-8552.
505 Giesy, J.P., Kannan, K., 2002. Perfluorochemical Surfactants in the Environment.
506 Environ. Sci. Technol. 36(7):146A-156A.
507 Han, D.M., Ma, Y.G., Huang, C., Zhang, X.F., Xu, H., Zhou, Y., Liang, S., Chen, X.J.,
508 Huang, X.Q., Liao, H.X., Fu, S., Hu, X., Cheng, J.P., 2019. Occurrence and
509 source apportionment of perfluoroalkyl acids (PFAAs) in the atmosphere in
510 China. Atmos. Chem. Phys., 19, 14107-14117.
511 Higgins, C.P., Luthy Richard G. 2006. Sorption of perfluorinated surfactants on
512 sediments. Environ. Sci. Technol. 40(23): 7251-7256.
513 Kim, S.K., Li, D.H., Kannan K. 2020. In situ measurement-based partitioning
514 behavior of perfluoroalkyl acids in the atmosphere. Environ. Eng. Res.
515 25(3):281-289.
516 Klaunig, J.E., Shinohara, M., Iwai, H., Chengelis, C.P., Kirkpatrick, J.B., Wang, Z.M.,
517 Bruner, R.H., 2015. Evaluation of the chronic toxicity and carcinogenicity of
518 perfluorohexanoic acid (PFHxA) in Sprague-Dawley rats. Toxicol. Pathol. 43 (2),
519 209-220.
520 Lei, Y.D., Wania, F., 2004. Is rain or snow a more efficient scavenger of organic
521 chemicals. Atmos. Environ. 38(22):3557-3571.
522 Leo, L.W.Y., Christopher, S., Mabury, S.A., 2017. Simultaneous analysis of
523 perfluoroalkyl and polyfluoroalkyl substances including ultrashort-chain C2 and
524 C3 compounds in rain and river water samples by ultra performance convergence
525 chromatography. J. Chromatogr. A. 1522(3): 78-85.

526 Li, J.F., He, J.H., Niu, Z.G., Zhang, Y., 2020. Legacy per- and polyfluoroalkyl
527 substances (PFASs) and alternatives (shortchain analogues, F-53B, GenX and
528 FC-98) in residential soils of China: Present implications of replacing legacy
529 PFASs. Environ. Int. 135:105419.
530 Lindstrom, A.B., Strynar, M.J., Delinsky, A.D., Nakayama, Shoji F., McMillan, L.,
531 Libelo, E.L., Neil, M., Thomas, L., 2011. Application of WWTP Biosolids and
532 Resulting Perfluorinated Compound Contamination of Surface and Well Water in
533 Decatur, Alabama, USA. Environ. Sci. Technol. 45(19):8015-8021.
534 Liu, B., Zhang, H., Yao, D., Li, J.Y., Xie, L.W., Wang, X.H., Wang, Y.P., Liu, G.Q.,
535 Yang, B., 2015. Perfluorinated compounds (PFCs) in the atmosphere of
536 Shenzhen, China: Spatial distribution, sources and health risk assessment.
537 Chemosphere. 138:511-518.
538 Liu, P., Li, Z., Li. B., Shi, G.L., Li, M.Q., Yu, D.Y., Liu, J.H., 2013. The analysis of
539 time-resolved optical waveguide absorption spectroscopy based on positive
540 matrix factorization. J. Colloid Interface Sci. 403:134-141.
541 Liu, W., Jin, Y.H., Quan, X., Dong, G.H., Liu, B., Wang, J., Wang, K., Yu, Q.L., Saito,
542 N., 2007. Investigation of PFOS and PFOA Pollution in Snow in Shenyang,
543 China Environ. Sci. 28(009):2068-2073. (In Chinese)
544 Liu, J.L., Shi, Y.G., Tang, N., Qin, R.X., Ma, Y., Xu, R.F., Wang, M.H., Zheng, J.,
545 2020. Pollution characteristics of seventeen per-and polyfluoroalkyl substances
546 in fish and sediments of Yangtze River Basin in Chongqing City, Environ. Chem.
547 (12): 3450-3461. (In Chinese)

548 Mee, 2019. Notice on Prohibition of the Production, Circulation, Use and Import and
549 Export of Persistent Organic Pollutants. Ministry of Ecology and Environment,
550 PRC.
551 Kwok, K.Y., Taniyasu, S., Yeung. L.W.Y., Murphy, M.B., Lam, P.K.S., Horri, Y.,
552 Kannan, K., Petrick, G., Sinha, R, K., Yamashita, N., 2010. Flux of
553 Perfluorinated Chemicals through Wet Deposition in Japan, the United States,
554 And Several Other Countries. Environ. Sci. Technol. 44(18):7043-7049.
555 Martínez-Moral, M.P., Tena, M.T., 2012. Determination of perfluorocompounds in
556 popcorn packaging by pressurised liquid extraction and ultra-performance liquid
557 chromatography–tandem mass spectrometry. Talanta. 101:104-109.
558 Paragot, N., Becanova, J., Karaskova, P., Prokes, R., Klanova, J., Lammel., G.,
559 Degrendele, C., 2020. Multi-year atmospheric concentrations of per- and
560 polyfluoroalkyl substances (PFASs) at a background site in central Europe.
561 Environ. Pollut. 265, 114851.
562 Pu, X., Li, Z.L., Zhang, Y., Gao, Y.H., Lv, P.J., Zhang, W.D., Zhai, C.Z., 2021.
563 Characterization of atmospheric circulation and transmission in Chongqing City
564 during ozone polluted days. China Environ. Sci. 41(01):18-27. (In Chinese)
565 Qi, Y.J., He, Z.S., Huo, S.L., Zhang, J.T., Xi, B.D., Hu, S.B., 2017. Source
566 apportionment of perfluoroalkyl substances in surface sediments from lakes in
567 Jiangsu Province, China: Comparison of three receptor models. J. Environ. Sci.
568 57: 321-328.
569 Sammut, G., Sinagra, E., Helmus, R., deVoogt, P., 2017. Perfluoroalkyl substances in

570 the Maltese environment - (I) surface water and rain water. Sci. Total Environ.
571 589(1):182-190.
572 Scott, B.F., Spencer, C., Mabury, S.A., Muir, D.C.G., 2006. Poly and perfluorinated
573 carboxylates in North American precipitation. Environ. Sci. Technol.
574 40(23):7167-7174.
575 Shan, G.Q., Chen, XW., Zhu, L.Y., 2015. Occurrence, fluxes and sources of
576 perfluoroalkyl substances with isomer analysis in the snow of northern China. J.
577 Hazard Mater. 299:639-646.
578 So, M.K., Miyake, Y., Yeung, W.Y., Ho, Y.M., Taniyasu, S., Rostkowski, P., Yamashita,
579 N., Zhou, B.S., Shi, X.J., Wang, J.X., Giesy, J.P., Yu, H., 2007. Perfluorinated
580 compounds in the Pearl River and Yangtze River of China. Chemosphere,
581 68(11):2085-2095.
582 Sun, D.C., Gong, P., Wang, X.P., Wang, C.F., 2018. Special distribution and seasonal
583 variation of perfluoroalkyls substances in Lhasa River Basin, China. China
584 Environ. Sci. 38(11):4298-4306. (In Chinese)
585 Taniyasu, S., Yamashita, N., Moon, H.B., Kwok, K.Y., Lam, P.K.S., Horii, Y., Petrick,
586 G., Kannan, K., 2013. Does wet precipitation represent local and regional
587 atmospheric transportation by perfluorinated alkyl substances. Environ. Int. 55:
588 25-32.
589 Wang, H.B., Zhang, L.M., Huo, T.T., Wang, B., Yang, F.M., Chen, Y., Tian, M., Qiao,
590 B.Q., Peng, C., 2020. Application of parallel factor analysis model to decompose
591 excitation-emission matrix fluorescence spectra for characterizing sources of

592 water-soluble brown carbon in PM2.5. Atmos. Environ. 223, 117192.
593 Wang, J.M., Pan, Y.Y., Shi, Y.L., Cai, YQ., 2011. Perfluorinated compounds in snow
594 from downtown of Beijing, China. SCIENTIA SINICA Chimica.
595 041(005):900-906. (In Chinese)
596 Wang, Y.M., He, L., 2020. The study on the scavenging effect of nighttime rainfall on
597 the atmospheric particulate matter in the Pearl River Delta. Environmental
598 pollution and prevention, 42(09):1075-1080. (In Chinese)
599 Wu, J., Jin, H.B., Li, L., Zhai, Z.H., Martin, J.W., Hu, J.X., Peng, L., Wu, P.F., 2019.
600 Atmospheric perfluoroalkyl acid occurrence and isomer profiles in Beijing,
601 China. Environ. Pollut. 255(1):113129.
602 Xiao, F., Halbach, T.R., Simcik, M.F., Gulliver, J.S., 2012. Input characterization of
603 perfluoroalkyl substances in wastewater treatment plants: source discrimination
604 by exploratory data analysis. Water Res. 46 (9), 3101-3109.
605 Yao, Y.M., Zhao, Y.Y., Sun, H.W., 2016a. The atmospheric distribution and seasonal
606 variation of volatile perfluoroalkyl substance precursors in Tianjin. Environ.
607 Chem. 2016, 35(7) :1329-1336. (In Chinese)
608 Yao, Y.M., Chang. S., Sun, H.W. Gan Z.W., Hu, H.W., Zhao, Y.Y., Zhang, Y.F., 2016b.
609 Neutral and ionic per- and polyfluoroalkyl substances (PFASs) in atmospheric
610 and dry deposition samples over a source region (Tianjin, China). Environ. Pollut.
611 212:449-456.
612 Young, A.S., Sparer-Fine, E.H., Pickard, H.M., Sunderland, E.M., Peaslee, G.F., Allen,
613 J.G., 2021. Per- and polyfluoroalkyl substances (PFASs) and total fluorine in fire

station dust. J. Expo. Sci. Environ. Epide. 31, 930-942.

Zhang, B., He. Y., Huang. Y.Y., Hong, D.H., Yao, Y.M., Wang, L., Sun, W.W., Yang, B.Q., Huang, X.F., Song, S.M., Bai, X.Y., Guo, Y.K., Zhang, T., Sun, H.W., 2020. Novel and legacy poly- and perfluoroalkyl substances (PFASs) in indoor dust from urban, industrial, and e-waste dismantling areas: The emergence of PFASs alternatives in China. Environ. Pollut. 263(Pt A): 114461.

Zhang, M., Tang, F.L., Yu, Y.Y., Xu, J.F., Chen, J.H., Yu, B., Zhou, S., Zhang, W., 2017. Perfluorinated Compounds in Snow from Downtown Hangzhou, China. Environ. Sci. 038(008):3185-3191. (In Chinese)

Zheng, Y., 2020. Contaminant Characteristics of Perfluorinated Compounds in Atmospheric of Typical Cities. Master Degree Dissertation. Qingdao University，China.

Zhou, Y.S., Tao, Y., Li, H. R., Zhou, T.T., Jing, T., Zhou, Y. K., Mei, S.R., 2016. Occurrence investigation of perfluorinated compounds in surface water from East Lake (Wuhan, China) upon rapid and selective magnetic solid-phase extraction. Sci. Rep. 6(1):38633.

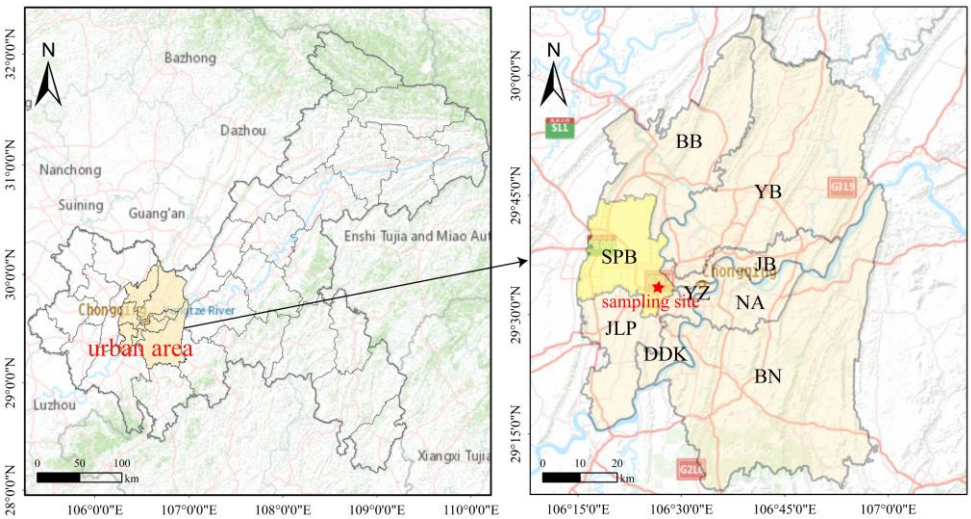

631

632 Figure 1 Sampling site in urban Chongqing.

633

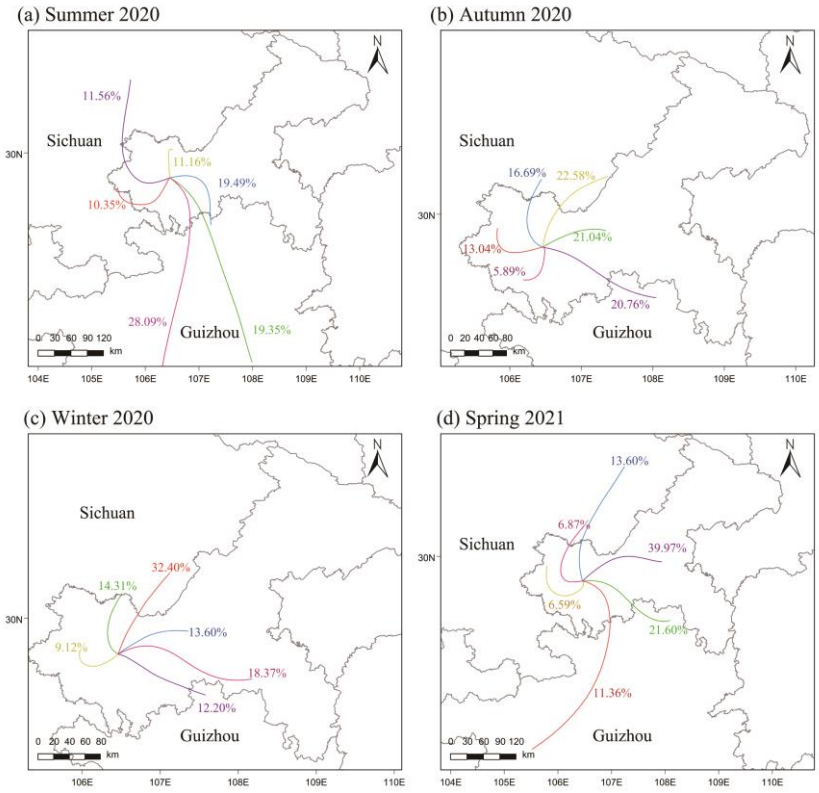

634

635 Figure 2 The clustered 24-hour air mass back trajectories from altitudes of 100 m

636 arriving at sampling site during the sampling period.

637

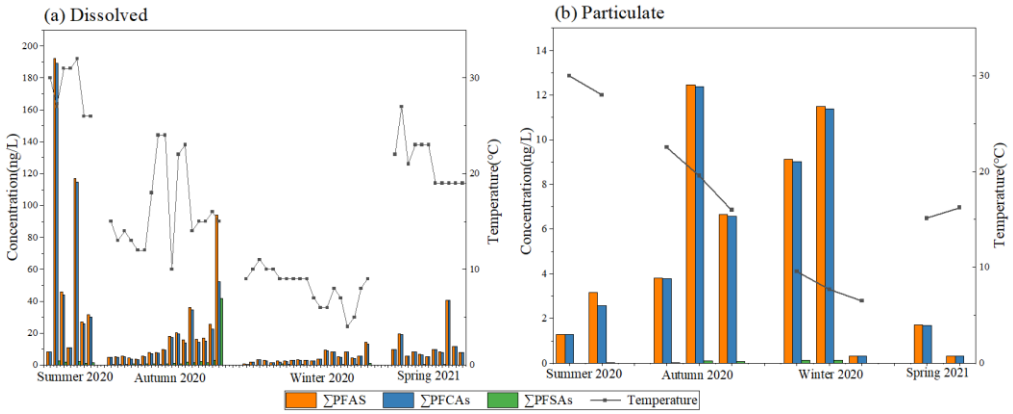

Figure 3 Seasonal variation of the concentrations of PFASs in the dissolved and particulate samples (colorful histogram), and the ambient temperatures (solid dot line).

643

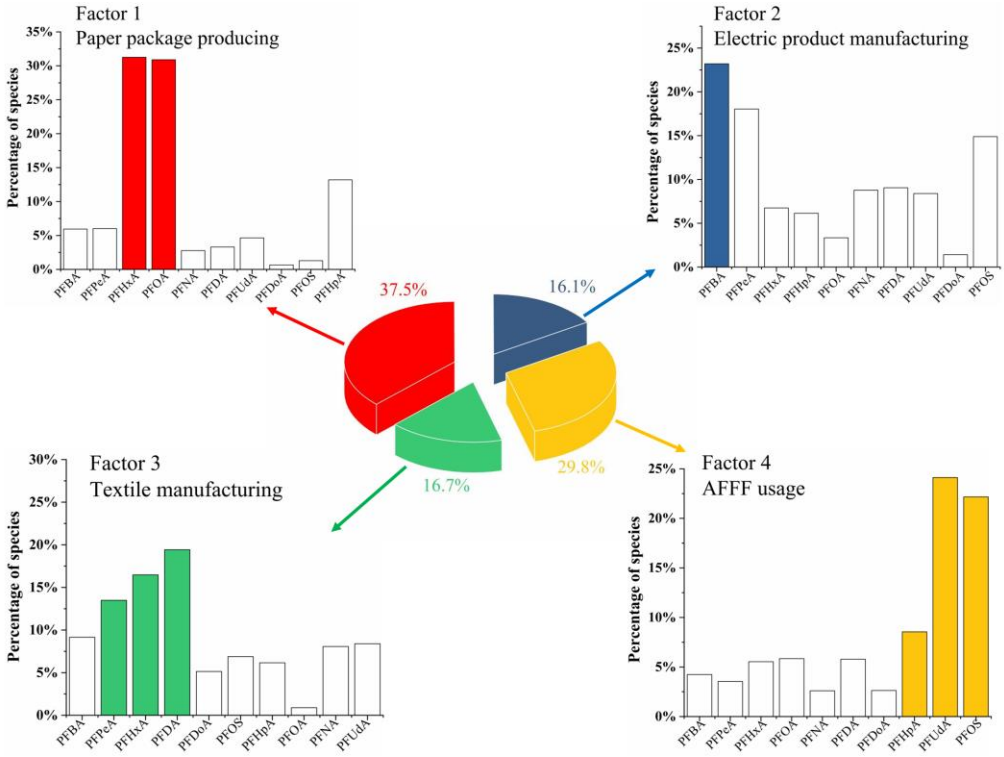

644 Figure 4 4-factor solution and their contributions on whole samples and PMF factor

645 profiles.

646

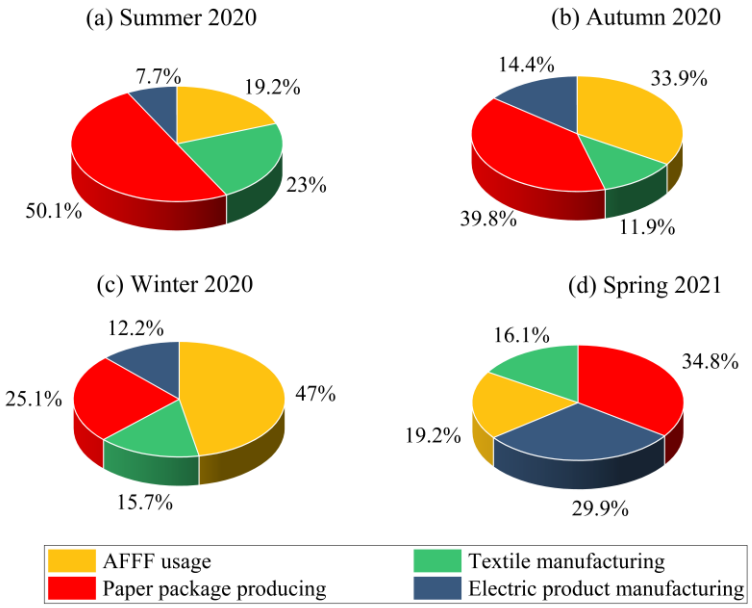

647

648 Figure 5 Contributions of the four sources to 9 PFASs in rainwater of urban

649 Chongqing over four seasons.

650 Table 1 Comparisons of the mean concentrations of selected PFASs (ng/L) in rainwater at Chongqing with other places worldwide.

Sampling	PFASs concentration: range (average)										
	ΣPFASs	PFOA	PFOS	PFBA	PFPeA	PFHxA	PFHpA	PFNA	PFDA	PFUdA	References
Hongkong (2006.06-2008.10)	-	0.20-0.41 (0.32)	<0.10-0.70 (0.32)	0.53-1.79 (1.02)	<0.05-0.62 (0.20)	<0.25-0.62 (0.35)	<0.25-15.7 (4.58)	0.13-044 (0.28)	0.14-0.31 (0.19)	0.04-0.19 (0.10)	Kwok et al., 2010
Beijing (2009.11)	0.47-7.94 (2.37)	nd*-2.96 (0.847)	0.038-4.76 (0.518)	-	-	-	0.057-0.558 (0.235)	0.055-2.16 (0.527)	nd-0.958 (0.139)	nd-0.208 (0.025)	Wang et al., 2011
Northern China (2013.01)	33.5-229 (93.7)	8.21-90.3 (30.64)	2.75-40.13 (13.03)	-	-	3.21-23.6 (11.1)	3.66-44.8 (16.4)	1.45-7.22 (4.25)	0.40-9.28 (2.66)	-	Shan et al., 2015
Hangzhou (2016.01)	2.85-35.1 (15.3)	2.15-23.0 (10.8)	nd-0.46 (0.23)	0.27-6.81 (2.40)	-	0.24-2.34 (0.83)	-	nd-0.41 (0.30)	-	-	Zhang et al., 2017
Beijing (2018.07-2018.10)	0.23-62.4	0.23-28.2	nd-6.30	nd-2.86	-	nd-2.86	nd-2.92	nd-2.40	nd-0.87	-	Zheng et al., 2020
Northern Italy (2007.10-2008.05)	-	0.04-9.3	0.1-3.3	nd-9.4	-	nd-1.9	nd-1.2	0.1-3.7	nd-7.5	-	Dreyer et al., 2010
Toronto (2012.10)	-	0.072	0.120	nd-0.12	<0.01-0.03	0.079	0.284	< 0.002	0.020	< 0.005	Leo et al., 2017
Maltese Islands (2015.08)	4.05	0.32	0.26	-	-	nd	0.29	0.53	2.65	-	Sammut et al., 2017
The Great Lakes (2018.05)	-	0.55	0.80	0.76	0.41	0.39	0.40	0.29	<0.2	-	Gewurtz et al., 2019
Chongqing (2020.07-2021.04)	0.9-191.3 (20.3)	0.2-121.2 (10.4)	nd-41.5 (1.2)	0.06-24.6 (2.4)	0.03-12.6 (1.2)	nd-19.7 (1.5)	0.01-11.6 (0.9)	0.01-10.1 (1.0)	nd-8.9 (0.5)	nd-8.9 (0.3)	This study

651 Table 2 The log K_d (cm^3/g) of 13 PFASs.

652

species	logK$_d$ 2020 summer	2020 autumn	2020 winter	2021 spring	average	SD
PFBA	9.3	9.0	9.0	7.5	8.7	0.8
PFPeA	8.9	9.0	9.1	7.6	8.7	0.7
PFHxA	10.0	10.0	10.3	7.7	9.5	1.2
PFHpA	9.5	9.3	9.9	7.6	9.0	1.0
PFOA	9.1	9.2	9.5	8.3	9.0	0.5
PFNA	9.0	8.2	6.9	6.8	7.7	1.1
PFDA	9.0	7.7	6.6	7.5	7.7	1.0
PFUdA	NA	7.2	9.5	7.5	8.1	1.2
PFDoA	NA	NA	7.4	7.7	7.6	0.2
PFHxDA	7.2	NA	8.6	5.6	7.2	1.5
PFBS	NA	NA	8.6	8.2	8.4	0.3
PFHxS	NA	8.4	7.7	7.2	7.8	0.6
PFOS	8.6	7.7	8.9	7.3	8.1	0.7

653 Table 3 Comparisons of wet deposition flux of PFAS at Chongqing with other places worldwide. (NA: not calculated as targeted species are

654 under method detection limit.)

region（time）	ΣPFAS	PFOA	PFOS	PFBA	PFPeA	PFHxA	PFHpA	PFNA	PFDA	PFUdA	References
This study (ng/m^2/season)											
2020 summer	1375.8	1007.3	54.9	81.9	61.2	54.8	48.8	32.6	13.6	1.2	-
2020 autumn	368.5	130.4	57.1	51.3	19.7	21.6	20.5	46.1	9.5	5.4	-
2020 winter	80.2	23.8	1.7	12.7	8.6	7.4	5.2	3.3	6.9	4×10^{-4}	-
2021 spring	211	104.6	1.1	0.03	12.3	36.9	16.3	7.5	2.2	0.2	-
Wet deposition flux (ng/m^2/day)											
This study	NA-175.5	NA-121.2	NA-41.5	7×10^{-8}-7.8	3×10^{-5}-12.6	NA -19.6	2×10^{-5}-11.6	6×10^{-6}-10.1	NA-2.9	NA-1.3	
Xiamen(2016)	872	170	240	NA	NA	170	130	120	42	-	Chen et al., 2019
Shenzhen(2016)	1162.7	690	83	94	130	12	110	34	9.7	-	
Hefei(2016)	595	48	280	87	60	57	20	25	18	-	
Chengdu(2016)	270.7	48	59	41	-	50	29	34	9.7	-	
Nanjing(2016)	446	100	160	1.0×102	50	70	40	20	6	-	
Northern Germany (2007.10-2008.05)	2.0-91	0.8-13.9	0.1-11.9	1.3-10.7	-	0.3-2.7	0.2-2.4	0.1-11.9	0.1-2.8	-	Dreyer, et a., 2010
Canada (1998-2003)	540-5158	3-726	-	6-295	-	6-441	12-386	1-789	-	-	Scott et al., 2006
Lake Ontario (2018.05)	6.8-36.8	2.0-5.0	3-5.5	2.2-5.2	0.1-4.1	0.4-3.9	0.3-4.2	1.0-4.2	NA-3.5	-	Gewurtz et al., 2019

655